PAPER

NJC
www.rsc.org/njc

Theoretical chemical contribution to the simulation of the L_{III} X-ray absorption edges of uranyl, neptunyl and osmyl hydrates and hydroxides

Christophe Den Auwer,*[a] Dominique Guillaumont,[a] Philippe Guilbaud,[a] Steven D. Conradson,[b] John J. Rehr,[c] Alexi Ankudinov[c] and Eric Simoni[d]

[a] *DEN/DRCP/SCPS, CEA Marcoule, 30207, Bagnols sur Cèze cedex, France*
[b] *MST Division, Los Alamos National Laboratry, MS G755, PO Box 1663, Los Alamos, NM 87545, USA*
[c] *Department of Physics, University of Washington, Seattle, WA 98195, USA*
[d] *Institut de Physique Nucléaire d'Orsay, Bat 100, 91405, Orsay cedex, France*

***Received* (in Montpellier, France) 2nd February 2004, Accepted 22nd April 2004**
First published as an Advance Article on the web 21st July 2004

XANES spectroscopy has long been used as a structural and electronic probe of a selected element. Phenomenological application of this technique to actinide cations has proved fruitful to characterize the actinide environment in both solid state and solution compounds. Although powerful XANES simulation codes have been developed, the use of such simulations in order to describe the valence orbitals of the actinide cation is still scarce. The very short life time of the core hole at the L_{III} edge as well as the low symmetry and large size of the coordination polyhedron are difficulties to be overcome in the analysis of the edge spectra. In this work, three simple molecules have been selected for their similar geometry that is typical of the trans dioxo actinyl compounds: $[UO_2(H_2O)_5]^{2+}$, $[NpO_2(H_2O)_5]^{2+}$, $[NpO_2(OH)_4]^{2-}$. Additional comparison with a transition metal, the osmyl cation $[OsO_2(OH)_4]^{2-}$, is also made. The cation L_{III} edges have been recorded and compared to edge calculations using FEFF8.2 code. This article is structured in two parts. In the first one, elaboration and optimization of a valid structural model cluster is carried out using molecular dynamics calculations. The influence of the water solvent molecules as well as the hydrogen atoms of the cations' first coordination sphere are discussed. In the second part, Amsterdam quantum chemical calculations have been carried out on the four clusters and molecular energy levels are qualitatively compared to the data obtained from calculated XANES spectra.

Introduction

The actinide elements, like their lanthanide homologues, possess a partially filled f valence shell. This electronic configuration gives them some specific properties with regards to the d block elements.[1] Among the actinide family, the actinyl cations possess specific chemical properties among which is the very short dioxo bond. Unlike the dioxo species of the transition metal series, the bond is invariably linear from uranium to americium. Theoretical, structural and spectroscopic investigations of actinyl adducts have been widely reported in the literature.[2–7] In particular, since many years, the optical properties of the uranyl cation, in relation with its speciation in solution, have been extensively studied.[8–12] Moreover, the uranyl electronic structure in condensed matter was extensively discussed using UV-Vis energy excitation or two-photon absorption,[13] on the basis of the absorption and emission spectra of hexavalent uranium. Nevertheless, a definitive interpretation according to these spectroscopic data has never been proposed. Up to now, the overall appearance of uranyl optical spectra has been interpreted considering the minor effect of the equatorial ligands compared to the two axial oxygen atoms. Indeed, these spectroscopic properties depend mainly on both the linear trans dioxo structure and the anomalously short U–O bond. Consequently, in a first approximation, although the actinide ions usually present a weak electron-phonon coupling, the fine structure of the low energy absorption spectrum is interpreted in terms of coupling of the O–U–O electronic transitions with the O–U–O symmetric stretching mode.[14] In the case of the actinyl species, this strong coupling is probably evidence of a charge transfer mechanism. The contribution of electron-electron repulsion, spin-orbit coupling and the crystal field (usually D_{5h} symmetry for aquo ion) are usually taken into account in the analysis and determination of the ordering of energy levels.[7,15–20] The main absorption and emission bands of the uranyl spectra are attributed to the transitions between the σ_u-HOMO and the 5f and 6d empty molecular orbitals accompanied by numerous vibronic side bands. Some of these features have been successfully fitted using the configurational coordinate diagram together with the time-dependent theory of electronic spectroscopy.[21] The presence of the ligands (equatorial or other) is taken into account through the crystal field and the electron-phonon coupling. Moreover the iono-covalency of the bonding and the charge transfer between uranium and axial oxygen atoms depend on the type of ligands (donor atom, for example) and on the structure of the actinyl complex. Recently, a mixed density functional theory and X-ray spectroscopic study of uranyl ion has been reported. It supports the valence orbital ordering obtained from optical spectroscopy using polarized oxygen K edge X-ray measurements.[6]

The use of X-ray absorption spectroscopy in the hard X-ray regime to investigate actinyl molecular adducts has been of increasing interest in the past decade. This is particularly true for species in solutions, when complementary speciation techniques such as optical and vibrational spectroscopies or quantum chemical calculations can be employed.[22–25] The energy position of the actinide L_{III} edges within the hard

DOI: 10.1039/b401607f

X-ray regime of the synchrotron spectrum, between 17 000 and 19 000 eV, is particularly convenient from the experimental point of view and allows measurement across multiple barrier confinement of the sample.[26,27] Accordingly, numerous studies that are based on L_{III} edge measurements discuss the formal oxidation state determination, coordination sphere geometry or valence orbital properties. It has been, for instance, well-reported that trans dioxo actinyl species are characterized by a well-defined multiple scattering contribution at about 15 eV above the edge maximum.[28–30] This contribution comes from the linear trans dioxo unit of the actinyl bipyramidal (tetra, penta or hexa) structure. The position and width of this shoulder depend on the difference between the equatorial bond length and the axial ones according to the ΔER^2 product (where ΔE is the difference between the resonance energy of the contributors at distance R and, say, the white line maximum). An octahedral symmetry leads to a significantly different edge shape with a low energy contribution that has been interpreted in the molecular orbital picture as coming from the low-lying t_{2g} orbital of the 6d's and in the multiple scattering picture as a triple scattering path within the octahedron.[31] On the contrary, actinide and lanthanide hydrates (based, for instance, on a tricapped trigonal prism for La[32]) in aqueous solution and at the formal oxidation state III exhibit an intense, featureless white line.[33,34] These examples show the sensitivity of the L_{III} edge to the polyhedron structure, despite the large broadening due to the short lifetime of the core hole states. Note also that a few studies at the L_I edge have also been reported.[29]

The X-ray absorption spectrum of a given element is commonly divided in two different regions, the pre-edge and edge region and the post-edge region, called EXAFS, which corresponds to significantly different processes.[35,36] In the edge region, low energy excited states are considered and transitions to bound states or quasi-bound states are often observed. In a simple one-electron molecular orbital (MO) picture, the authorized LUMO or partially vacant valence orbitals are probed by the photoelectron according to the dipolar transition rule. Quadrupolar transitions or phonon coupling can also contribute to the edge as observed for several transition metals. Within the one-electron multiple scattering picture, both the absorption coefficient μ and the angular momentum (l)-projected density of states (DOS) ρ have smooth atomic backgrounds modulated by the oscillating function χ.[28] Transitions to bound or quasi-bound states resulting from mixing with continuum states occur below or around the vacuum level. Above the continuum threshold, in the EXAFS regime, the final one-electron state belongs to the continuum and the spectrum is dominated by constructive or destructive interferences contained in χ. According to the dipole approximation of the Fermi Golden rule, the transitions of interest in this paper are the following at the L_{III} edge: $2p^65f^06d^0 \rightarrow 2p^55f^06d^1$ for U(VI); $2p^65f^16d^0 \rightarrow 2p^55f^16d^1$ for Np(VI) and $2p^64f^{14}5d^0 \rightarrow 2p^54f^{14}5d^1$ for Os(VI).

In this paper, we discuss the calculated and experimental X-ray absorption edge spectra of structurally related small actinyl molecules in aqueous solution. Edge calculations are based on the FEFF8.2 code using a self-consistent real-space Green's function formalism.[37] A tentative interpretation of the edge using the electronic properties of the metal cation valence MO and Amsterdam density functional (ADF) calculations is proposed. The paper is thus formally formatted into two parts: a first one devoted to the elaboration of a valid structural model for each cluster in aqueous solution using molecular dynamics (MD) calculations, a second one discussing the comparison between the calculated spectrum and *ab initio* quantum chemistry calculations. Four molecular species have been selected: uranyl(VI) and neptunyl(VI) cations in perchloric solution, forming the pentagonal bipyramid hydrates $[UO_2(H_2O)_5]^{2+}$ and $[NpO_2(H_2O)_5]^{2+}$; neptunyl(VI) cation in strong basic solution forming the tetragonal bipyramid hydroxide $[NpO_2(OH)_4]^{2-}$ and osmyl(VI) cation forming an insoluble hydroxide $[OsO_2(OH)_4]^{2-}$ compound in aqueous solution with a tetragonal bipyramid structure.

In order to focus the discussion towards the sensitivity of the edge spectrum to fine structural and electronic changes within the four species, all the cations are present at the same formal oxidation state VI. The osmyl trans dioxo cation brings up an interesting comparison between the 5f and 5d blocks and the role of the corresponding valence orbitals. The four molecular species can be divided in two types of bipyramidal molecular skeletons [referred to in the following as $(MO_2)O_5$ for the hydrates and $(MO_2)O_4$ for the hydroxides], as shown in Chart 1.

Experimental

Sample preparation

$[UO_2(H_2O)_5]^{2+}$ was prepared according to the literature[38] in perchloric solution (0.01 M). $[NpO_2(H_2O)_5]^{2+}$ was prepared in perchloric solution (1 M).[39] $[NpO_2(OH)_4]^{2-}$ was prepared in aqueous solution of trimethyl ammonium hydroxide (TMA-OH; 2.5 M).[39] $K_2[OsO_2(OH)_4]$ was prepared from OsO_4 (0.16 M, Acros Inc.) dissolved in potassium hydroxide aqueous solution (1.6 M). Reduction and precipitation was obtained upon dropwise addition of EtOH. The deep red precipitate of $K_2[OsO_2(OH)_4]$ was washed with water and ethanol.[40]

Data acquisition and data treatment

All XANES data have been recorded at the Stanford Synchrotron Radiation Laboratory (SSRL) on the 11–2 beam line. SPEAR synchrotron ring runs at 3.0 GeV with an optimal current of 100 mA. A nitrogen-cooled double-crystal Si220 monochromator with no focusing device was used, giving an experimental resolution of $\Delta E = 5$ eV at 17 000 eV. The monochromator was energy calibrated with a Y foil (17 052.0 eV) for uranium, a Zr foil (18 014.0 eV) for neptunium and a W foil (10 206.8 eV) for osmyl. Measurements were carried out in fluorescence mode with a Ge 30 element detector and an I0 ionization chamber.

The presented data have all been energy shifted towards the second derivative zero value (inflexion point). XANES spectra have been treated with ARTEMIS code using the AUTOBK normalization procedure.[37] Absorption and dead time corrections have been made by calibrating the contribution of the EXAFS first neighbor intensity to 2 (2 axial oxygen atoms). The structures of the 4 molecular skeletons (*i.e.*, the metallic cation and the axial and equatorial oxygen atoms) have been idealized with a perfect bipyramidal geometry. All the distances used for the calculations have been taken from EXAFS measurements: $[UO_2(H_2O)_5]^{2+}$: 2 O @ 1.75 Å and 5 O @ 2.42 Å;[38] $[NpO_2(H_2O)_5]^{2+}$: 2 O @ 1.75 Å and 5 O @ 2.42 Å;[27] $[NpO_2(OH)_4]^{2-}$: 2 O @ 1.82 Å and 4 O @ 2.21 Å;[41] $[OsO_2(OH)_4]^{2-}$: 2 O @ 1.75 Å and 4 O @ 2.03 Å (EXAFS best fit parameters obtained with FEFF8.2 phases and amplitudes).

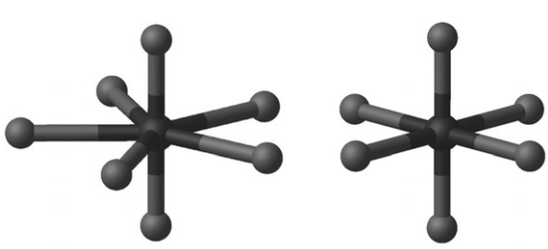

$[MO_2(H_2O)_5]^{2+}$ (M=U,Np) $[MO_2(OH)_4]^{2-}$ (M=Np,Os)

Chart 1

Molecular dynamics calculations

Molecular dynamics simulations have been performed with the AMBER 6.0 package,[42,43] using the following representation of the potential energy:

$$E = \sum_{\text{bonds}} K_r(r - r_{\text{eq}})^2 + \sum_{\text{angles}} K_\theta(\theta - \theta_{\text{eq}})^2 + \sum_{\text{dihedrals}} V_n[1 + \cos(n\phi - \phi_0)] + \sum_{i=1}^{N-1}\sum_{j>i}^{N}\left[\frac{A_{ij}}{R_{ij}^{12}} - \frac{B_{ij}}{R_{ij}^{6}} + \frac{q_i q_j}{R_{ij}}\right]$$

Due to the difficulties related to the representation of actinide cations with an empirical force field, very few molecular dynamics simulations have been performed for these cations in solution. Some aqueous MD simulations using this energy representation have already been performed in order to reproduce complexation $\Delta\Delta G$ differences for UO_2^{2+} and its complexes with crown ether, calixarene, CMPO or $R_3P{=}O$ ligands in water solutions.[44–48] More recent studies related the development of a more sophisticated force field including both polarization and charge transfer to model uranyl-cation–water clusters.[5] Nevertheless, there is to date no published MD simulations concerning other actinide cations. Empirical parameters for both Np and Os cations are unavailable. Because the aim of this study is the structural determination of both the hydrogen atoms of the first coordination sphere and the surrounding water molecules, each of the 4 studied systems have been considered as rigid idealized bipyramid skeletons obtained by EXAFS measurements. U, Np and Os dioxo cations have all been modelled using charges and parameters from previous adjustments done for aqueous phase simulations on UO_2^{2+}.[44,46] The net charge difference between U, Np and Os in their "yl" form being quite small, there should be no significant effect from electrostatic interactions with water molecules in the cation second coordination sphere. Hydrogen atoms bonded to oxygen of the metal first coordination sphere (water or hydroxide hydrogen atoms) were added and allowed to move during the calculations. Charges on the hydroxides have been derived from electrostatic potential calculation using Gaussian98[49] and the RESP[50] method. Each of the 4 previously defined molecular skeletons was then immersed at the center of a cubic (37 Å^3) box containing around 1800 explicit TIP3P water molecules, with periodic boundary conditions. After a 1000 step geometry optimization, systems were equilibrated for 20 ps and a 700 ps molecular dynamics simulation at 300 K was achieved for data acquisition. These simulations have been performed using a 0.001 ps time step, with a 15 Å cut-off and applying the Particle Mesh Ewald algorithm.[51] In the case of UO_2^{2+} (for which parameters are available), molecular dynamics simulations have also been performed without any constraints on the molecular skeleton for comparison with the results obtained with the frozen systems.

Quantum chemistry calculations

Quantum chemistry calculations have been performed on $[UO_2(H_2O)_5]^{2+}$, $[NpO_2(H_2O)_5]^{2+}$, $[NpO_2(OH)_4]^{2-}$ and $[OsO_2(OH)_4]^{2-}$ clusters. The electronic and geometrical structures of the complexes have been calculated using density functional theory (DFT) with the Amsterdam density functional (ADF) program package.[52–54] Relativistic effects have been considered by the zeroth-order regular approximation (ZORA)[55–57] Spin-orbit effects have not been taken into account. Uncontracted triple-ζ Slater type valence orbitals with one set of polarization functions were used for all atoms. The frozen-core approximation was used where the core density was obtained from four-component Dirac–Slater calculations on all the atoms and kept frozen during molecular calculations. $1s^2$ core electrons were frozen on oxygen. The valence space of the heavy elements includes 5s, 5p, 5d, 4f, 6s shells of osmium and 6s, 6p, 6d, 5f, 7s shells of actinides (uranium, neptunium). The density functional consists of a local density part using the parameterization of Vosko, Wilk, and Nusair and exchange-correlation gradient corrected parts of Perdew.[58]

A comparison of calculated and experimental geometrical bond distances is given in Table 1. Calculated bond distances are slightly larger than experimental values, from 0.02 to 0.04 Å for actinyl and osmyl distances, and from 0.04 to 0.07 Å for metal–oxygen (equatorial) distances. Uranyl and neptunyl complexes have been the subject of several quantum chemistry studies and previous calculations at the DFT level with relativistic effective core potentials give 1.75 Å for uranyl distance in $[UO_2(H_2O)_5]^{2+}$[59] and 1.83 Å for the neptunyl distance in $[NpO_2(OH)_4]^{2-}$.[25] The agreement of the present calculation with experimental as well as with previous theoretical studies is correct.

The calculations give different conformations between $[NpO_2(OH)_4]^{2-}$ and $[OsO_2(OH)_4]^{2-}$ clusters. In the neptunyl complexes, the most stable conformation corresponds to OH^- groups bent out of the equatorial plane whereas in the most stable conformation of osmyl complexes, OH^- groups lie in the equatorial plane.

XANES calculations

The FEFF8.2 code[37] has been used for all the XANES simulations with similar calculation parameters: self consistency and full multiple scattering sphere up to the first water solvent molecule (between 4.1 and 4.3 Å depending on the cluster), no additional broadening from the imaginary part of the self energy. In order to take into account the global charge of the complex, partial ionization of each atom of the first coordination sphere (given here as fraction of electron counts) has been applied with values derived from the quantum chemical charge calculations (Mulliken analysis). $[UO_2(H_2O)_5]^{2+}$ and $[NpO_2(H_2O)_5]^{2+}$: U, Np = −0.48, O = −0.10, H = +0.07; $[NpO_2(OH)_4]^{2-}$: Np = −0.42, O = −0.16, H = +0.04; $[OsO_2(OH)_4]^{2-}$: Os = −0.40, O = −0.16, H = +0.04. These values have been arbitrarily set to a fixed fraction of the calculated charge in order to best match the experimental spectra. Note that: (i) the same fraction has been used for all the calculations, (ii) a small variation (±20%) of these values does not affect the spectrum shape but shifts the edge value to low energy, in agreement with a decrease of the cation charge.

Ground state density of states (DOS) calculations and population analysis have been carried out with the same code parameters (NOHOLE card).

Results and discussion

Optimization of the molecular structural model

The information included in the XANES spectrum has long been used as a structural probe around the central actinide cation.[28,33,60] Benfatto *et al.* have also discussed the relation

Table 1 Metal–oxygen bond distances (Å) in $[MO_2(H_2O)_5]^{2+}$ and $[MO_2(OH)_4]^{2-}$ complexes

	$M–O_{oxo}$		$M–O_{equatorial}$		
	Calcd	Exptal	Calcd	Exptal	Ref.
$[UO_2(H_2O)_5]^{2+}$	1.77	1.75	2.49	2.42	38
$[NpO_2(H_2O)_5]^{2+}$	1.76	1.74	2.47	2.42	27
$[NpO_2(OH)_4]^{2-}$	1.86	1.82	2.29	2.25	41
$[OsO_2(OH)_4]^{2-}$	1.78	1.75	2.09	2.03	This work

between local structure and XANES.[61] Conversely, the *ab initio* calculation of XANES spectra must be based on a model cluster that defines the best structural model of the compound under investigation. The optimization of this model is at the starting point of obtaining reliable calculated spectra. Two components can be schematically considered in the definition of a model cluster. The first one, according to the multiple scattering approach, defines the adequate position of the scattering atoms in space and the inclusion of enough atoms in the calculation. The second component deals with the potential calculation of each scattering atom and the difficulty of dealing with a finite cluster size. The first component is in most cases easily optimized starting with an X-ray or neutron diffraction structure in the solid state, although light scattering atoms such as hydrogen are usually difficult to localize by X-ray diffraction. However, inclusion of hydrogen atoms as significant contributors has been discussed by Merkling *et al.* and references therein[62] and has generally been found to be negligible. In the case of species in solution, the model cluster should represent, at best, an average of all the possible conformations. It can be based on assumptions derived from solid state structures or from molecular structures obtained by either theoretical chemistry[25,41] or other spectroscopic techniques. Inclusion of dynamical effects in the solution or solvent effects derived from computer simulations have been reported mainly for transition metals[62–64] but the use of such a procedure for actinide cations is rarer. The second component often depends on the structural approximations (inclusion of hydrogen atoms, cluster size and border effects, global charge borne by the molecule if needed) as well as the model of the potential used in the calculation.[62]

As mentioned in the Introduction, the L_{III} edges of uranyl, neptunyl and plutonyl adducts has been relatively well described in the literature, often based on a series of model solid state compounds.[30,33] However very few of these studies are devoted to molecules in solution. Three of the four molecular structures considered in this article are solvent adducts: $[UO_2(H_2O)_5]^{2+}$, $[NpO_2(H_2O)_5]^{2+}$ and $[NpO_2(OH)_4]^{2-}$. In order to account for the solvent part beyond the first coordination sphere, an approach using MD calculations has been performed for these systems in aqueous solution, leading to a sampling for both the first sphere hydrogen atoms and the surrounding water molecules around the actinyl molecular skeleton [the term "molecular skeleton" $(MO_2)O_5$ or $(MO_2)O_4$ (M = U, Np, Os) referring to the first coordination sphere structure excluding the hydrogen atoms]. Note that in the rest of the text the so-called first coordination sphere includes the two axial oxygen atoms and the four or five equatorial molecules (H_2O, OH^-) that are directly linked to the metallic cation. The so-called second coordination sphere includes the water molecules directly hydrogen bonded to the first coordination sphere. The fourth adduct, $[OsO_2(OH)_4]^{2-}$, is insoluble in aqueous solutions. At this point of the study, only the local order around the osmium atom has been determined by EXAFS measurements. Consequently, only the first coordination sphere has been taken into account in the model cluster with the positions of the hydrogen atoms derived from the quantum chemical calculations (see below). One of the major difficulties lies in obtaining suitable parameters for U and Np cations. In fact, except for UO_2^{2+}, there are, to our knowledge, no parameters to account for these cations in solution using an empirical force field and an explicit representation of the solvent. Since the aim of this study is the evaluation of first sphere hydrogen atoms and solvent structure effects for the three cations, simulations have been performed with skeletons allowing both first sphere (water or hydroxide) hydrogen atoms and all water molecules to move during the simulation. For these studied systems six molecular structures have been taken as instantaneous snapshots at regular time intervals during the MD simulations. These structures include the cation, its first coordination sphere, and all the water molecules having at least one atom included within 6 Å around the cation. Table 1 compares the structural data obtained from EXAFS with ADF calculations. Agreement on the distances is satisfactory although the average discrepancy for the equatorial ones (0.07 Å) is larger than for the axial ones (0.03 Å). Indeed, a better agreement is expected for the description of more covalent bonds, such as the axial ones, with respect to the more electrostatic bonding mode of the equatorial ligands.

Fig. 1 shows the molecular cluster resulting from one snapshot after 75 ps for $[UO_2(H_2O)_5]^{2+}$. Fig. 2 compares the experimental L_{III} edge of $[UO_2(H_2O)_5]^{2+}$ with 6 XANES calculations based on clusters obtained from the 6 snapshots (with frozen skeletons). Qualitatively, all the calculations reproduce the XANES features: the strong white line A, shoulder B attributed to the multiple scattering contribution of the trans dioxo unit and shoulder C (even if it is less intense in the simulation than in the experimental spectrum). Although some differences appear between each calculation corresponding to each snapshot, the broad character of the edge spectrum precludes the selection of one preferred conformation over another one by comparison with the experiment. The spectrum obtained when averaging the 6 calculations (which should represent the averaged conformation of the molecule in water) is indeed in very good agreement with the experiment. Before discussing the influence of the molecular conformation on the calculated edge, the scattering contributions from the successive coordination spheres around the uranium cation have been tested.

In Fig. 3 different patterns for the calculation of the edge of $[UO_2(H_2O)_5]^{2+}$ are compared. All the patterns are based on one molecular dynamics snapshot after 100 ps. Patterns 1 and 2 correspond to the inclusion of all the molecules up to 6 Å for the calculation of the atomic potentials. The scattering contributions from the solvent molecules (beyond the first coordination sphere) have been accounted for in pattern 1, whereas they have been omitted in pattern 2 (the calculation of the potentials being identical). No visible differences appear on the edge spectrum. In pattern 3, the scattering contribution from the hydrogen atoms of the first coordination sphere was also removed. Again, no clear differences can be observed. This result is in agreement with the conclusions of Merkling *et al.* on the edge spectra of Cr^{3+} and Rh^{3+},[62] suggesting that the scattering contributions are negligible for atoms beyond the first coordination sphere. It also agrees with some of the present authors' previous calculations on neptunyl cations.[65] However, as represented in pattern 4, exclusion of the hydrogen atoms in the atomic potential calculation of the molecular skeleton leads to a significant modification of the spectrum. Similarly, removal of all the water molecules beyond the first coordination sphere for both the scattering and the potential calculations (pattern 5) affects dramatically the calculated spectrum. To summarize, scattering contributions beyond the first coordination sphere as well as scattering contributions from the hydrogen atoms of the first coordination sphere are negligible. However, inclusion of at least two coordination spheres seems necessary to obtain a set of reliable atomic potentials for the molecular skeleton. This suggests, as shown in Fig. 2, that the modifications of features A and B from one snapshot to the next one are related to the modification of the skeleton atomic potentials. This modification is not caused by the skeleton itself (frozen option) but by the fluctuations of the hydrogen atoms as well as the water molecules.

In order to discuss this point, Fig. 4 presents the radial distribution functions (RDF) centered on uranium of both oxygen and hydrogen atoms of the first coordination spheres (up to 5 Å from U) for each snapshot. In the "frozen skeleton" mode, 2 oxygen atoms are represented at the lowest distance at 1.7 Å ("yl" oxygen atoms) and 5 are represented at 2.4 Å. The first distribution set of hydrogen peaks, between 3 and 3.5 Å, corresponds to the first coordination sphere atoms,

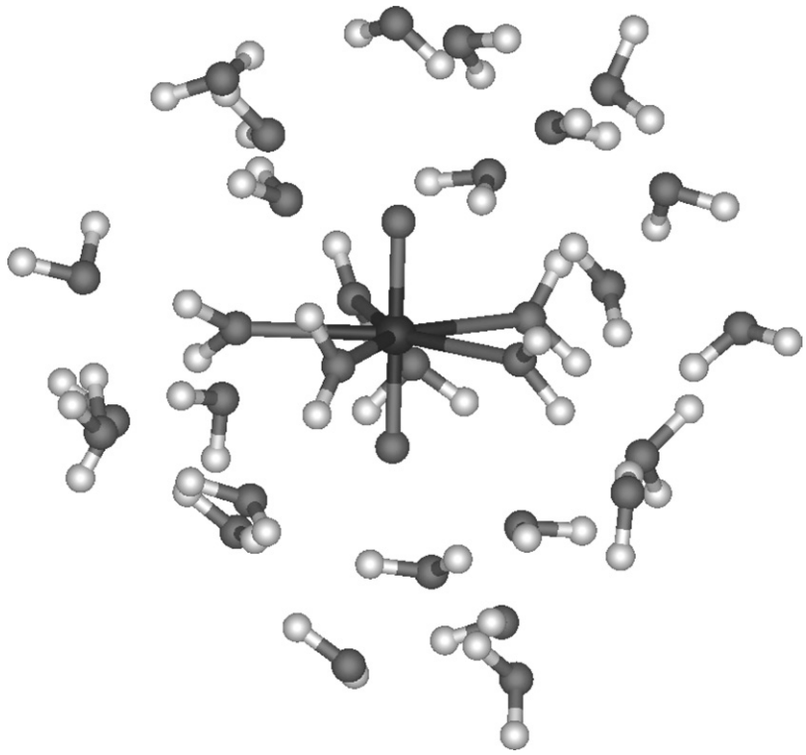

Fig. 1 Representation of the model cluster of $[UO_2(H_2O)_5]^{2+}$ in water resulting from one molecular dynamics snapshot (75 ps).

that is to the water molecules directly bonded to the uranium cation. The following hydrogen and oxygen sets, beyond 3.7 Å, correspond to the second sphere and further water molecules (23 to 27 water molecules between 4 and 6 Å). A qualitative comparison between the edge spectra and the radial distribution function shows that the closer the oxygen atom from at least one solvent molecule to the cation, the less intense is the calculated edge white line. The two limits are the 75 ps snapshot [most intense white line and $d(U–O_{wat}^{min}) = 4.07$ Å] and the 100 ps snapshot [less intense white line and $d(U–O_{wat}^{min}) = 3.76$ Å]. This suggests that the higher the density of water molecules close to the first coordination sphere, the less intense is the white line. There is, at this point of the study, no experimental evidence to corroborate the calculated result. One possible explanation is the following: the higher the anisotropic water distribution close to the uranyl cation, the higher the polarization of the first coordination sphere and the lower the symmetry around the cation, resulting in a decrease of the white line intensity. This effect is, however, small in magnitude. ADF calculations have been performed on the two limit snapshots (75 and 100 ps) and no significant difference has been observed in the electronic structure (composition and relative energy position of the molecular orbitals).

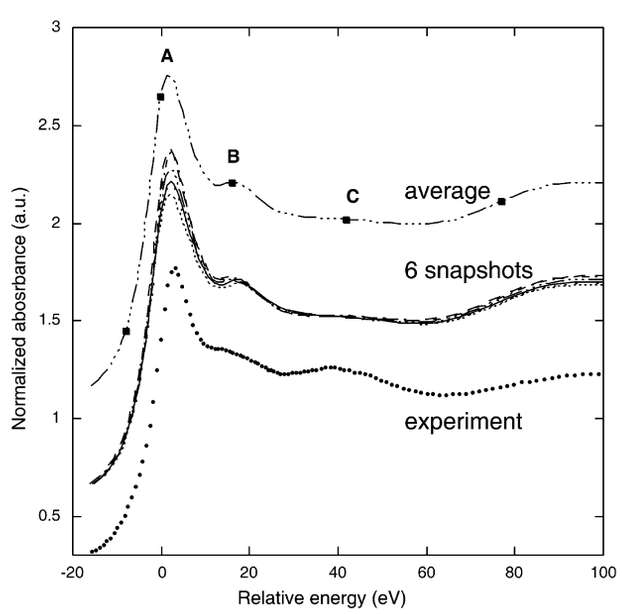

Fig. 2 Experimental and calculated L_{III} edge spectra of $[UO_2(H_2O)_5]^{2+}$. The 6 calculated edge spectra are based on MD calculations (frozen skeleton) according to 6 snapshots (— - - - — 50 ps; — — — 75 ps; - - - - - - 100 ps; - - - -125 ps; ——— 150 ps; — - — - — 175 ps). The average of the 6 spectra is also presented. For clarity, the experimental and calculated spectra have been shifted on the ordinate.

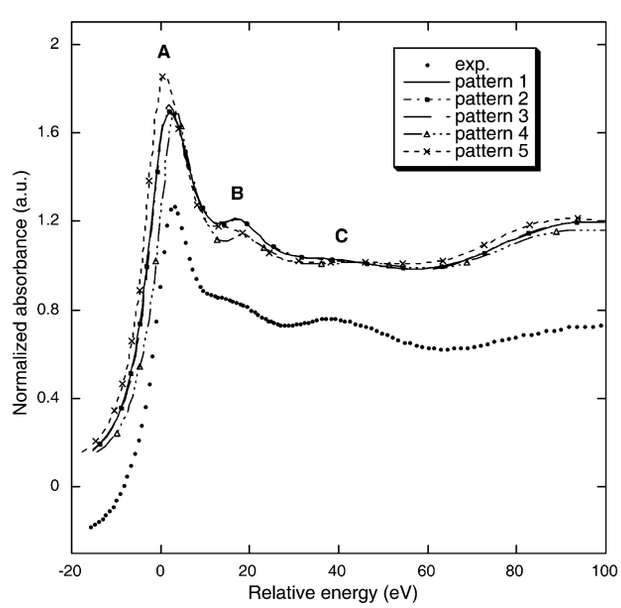

Fig. 3 Experimental and calculated L_{III} edge spectra of $[UO_2(H_2O)_5]^{2+}$. The 5 calculations correspond to one cluster (based on one MD snapshot after 100 ps) calculated with different potential and scattering patterns as described in the text. For clarity, the experimental and calculated spectra have been shifted on the ordinate.

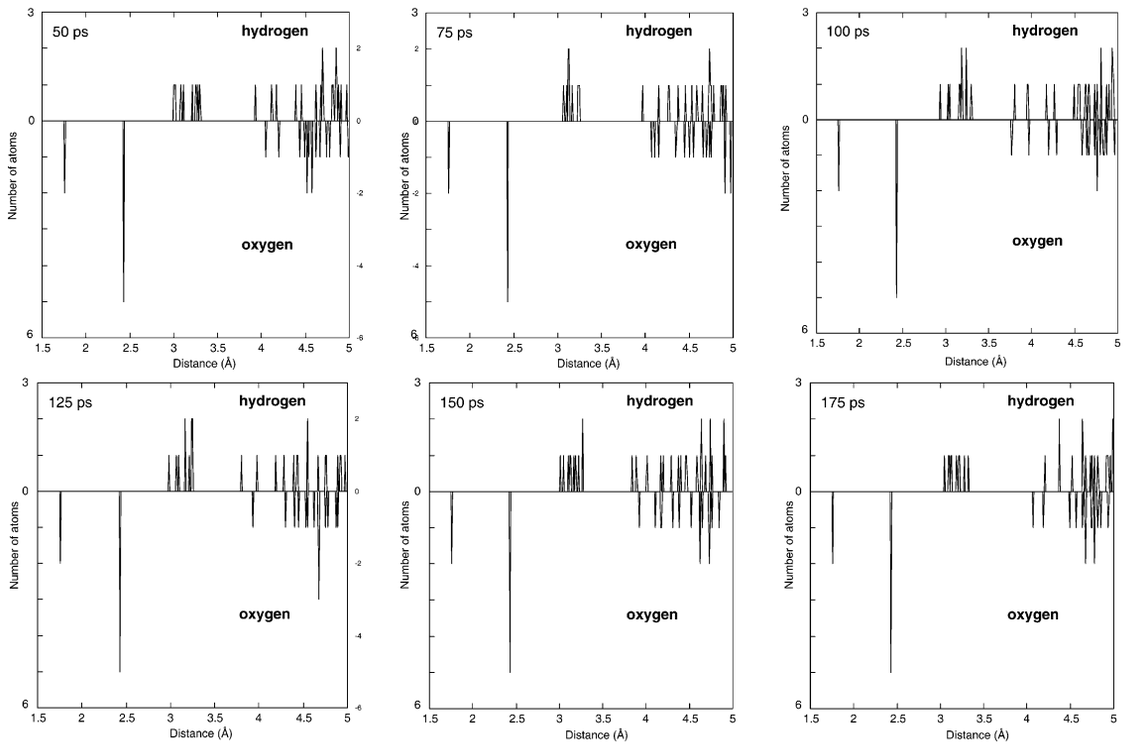

Fig. 4 Radial distribution functions of both hydrogen and oxygen atoms around the uranium cation in $[UO_2(H_2O)_5]^{2+}$. Each radial distribution function corresponds to one molecular dynamics snapshot (frozen skeleton) at the indicated time.

Fig. 5 also shows the relative importance of the first coordination sphere with regards to the second and third ones on the edge spectrum of $[UO_2(H_2O)_5]^{2+}$. It compares two sets of calculations based on the frozen and optimized skeleton options: with the optimized skeleton, the variations of the white line intensity and position are, as expected, far larger. This corroborates the previous assessments about the importance of the first coordination sphere in the build-up of the edge spectrum. The optimized skeleton option creates a series of snapshots with significant distortion of the first coordination spheres between each snapshot. The net result is a small dumping of the average white line intensity with respect to the frozen skeleton option. This difference should become negligible as a larger number of snapshots are taken into account in the calculation of the average. Nevertheless, their similarity shows that the overall influence of the method used for the computer simulations (frozen skeleton) is negligible when enough conformations (here 6 snapshots) are taken into account.

Fig. 6 shows the L_{III} edges of neptunyl in both acidic ($[NpO_2(H_2O)_5]^{2+}$) and basic ($[NpO_2(OH)_4]^{2-}$) aqueous solutions. The structural distortion of the molecular skeleton from acidic to basic media corresponds to an elongation of 0.07 Å of

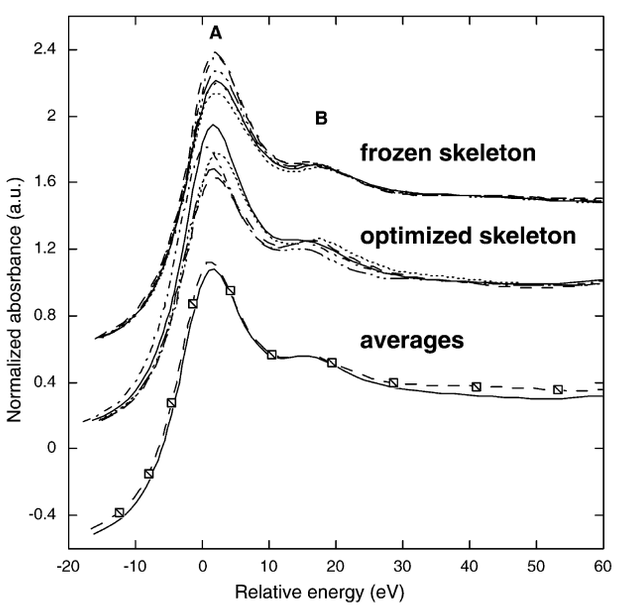

Fig. 5 Comparison between the edge calculations based on MD with frozen skeleton (—·--·— 50 ps; ———— 75 ps; ------ 100 ps; - - - -125 ps; ——— 150 ps; —·—·—· 175 ps) and optimized skeleton (—·--·— 50 ps; ———— 75 ps; ------ 100 ps; ——— 150 ps; —·—·—· 175 ps). For both cases, the averages (dashes with squares = frozen; solid line = optimized) are also compared. For clarity, each set has been shifted on the ordinate.

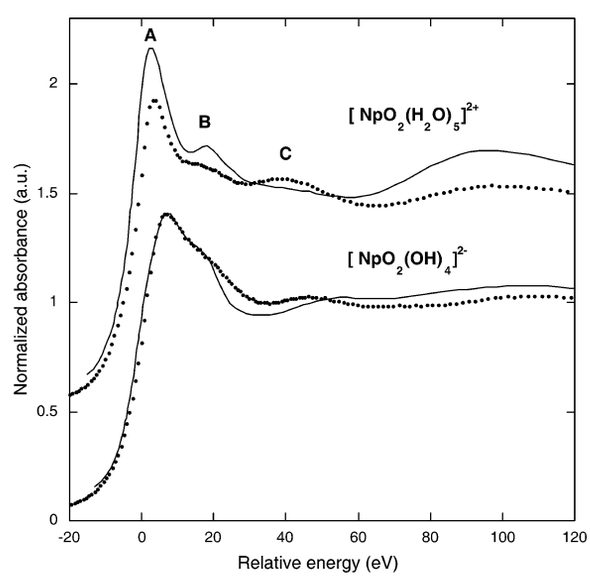

Fig. 6 Experimental (points) and calculated (solid line) L_{III} edge spectra of $[NpO_2(H_2O)_5]^{2+}$ (shifted on the ordinate) and $[NpO_2(OH)_4]^{2-}$. Both calculations are based on one MD snapshot (100 ps).

the axial distances and a contraction of 0.21 Å of the equatorial distances.[27, 41] Comparison of the corresponding experimental L_{III} edges shows that this deformation leads to dramatic changes in the edge spectrum:[60] strong differences in the intensity of A, shifts of B and C in the spectrum of $[NpO_2(H_2O)_5]^{2+}$ compared to $[NpO_2(OH)_4]^{2-}$. These differences are well-reproduced with both calculations using a cluster obtained from one MD snapshot (after 100 ps). Note that the same FEFF8.2 parameters have been used here as for the calculation of the spectrum of $[UO_2(H_2O)_5]^{2+}$. A comparison with Fig. 2 shows that the spectra of $[UO_2(H_2O)_5]^{2+}$ and $[NpO_2(H_2O)_5]^{2+}$ are very comparable due to the similarity of both skeletons. The strong differences observed in the edge spectrum of $[NpO_2(OH)_4]^{2-}$ confirm that the geometry of the first coordination sphere plays a major role in the shape of the edge. As described for the uranium edge, the position of feature B with respect to A is indicative of the axial Np–O distance. In $[NpO_2(OH)_4]^{2-}$, B is shifted to lower energies compared to $[NpO_2(H_2O)_5]^{2+}$, in agreement with a larger axial distance for the hydroxide with respect to the hydrate. The identity of the product ΔER^2 is indeed verified within the measurement error: $\Delta ER^2 = 12.5\ (\text{eV}) \times 1.75\ (\text{Å}^2) = 38$ for $[NpO_2(H_2O)_5]^{2+}$; $\Delta ER^2 = 10.0\ (\text{eV}) \times 1.82\ (\text{Å}^2) = 33$ for $[NpO_2(OH)_4]^{2-}$. Conversely, a careful analysis of the edge shape and feature positions may lead to reliable structural information about the near structure around the actinide cation.

Finally, Fig. 7 presents both experimental and calculated L_{III} edge spectra of osmyl hydroxide, $[OsO_2(OH)_4]^{2-}$. The geometry of the molecular skeleton exhibits a strong distortion compared to the ones of $[NpO_2(OH)_4]^{2-}$ and $[NpO_2(H_2O)_5]^{2+}$: : an axial distance of 1.75 Å and very short equatorial distances of 2.03 Å. Due to the lack of structural information about the bulk in this material, the isolated molecule in vacuum has been considered and the quantum chemistry calculation of the structure is in a fairly good agreement with the EXAFS results (see Table 1). The most stable conformation corresponds to a structure with 4 OH^- groups in the equatorial plane. Comparison with the experimental spectra of Fig. 7 shows a strong increase of white line A compared to the actinyl case. This point is discussed in the next section. Feature B is attributed to the multiple scattering contribution of the two axial oxygen atoms, as suggested by the calculation carried out in the single scattering mode. Feature C has not been fully attributed and it is poorly reproduced by the simulation. This discrepancy is attributed to the limited size of the model cluster (limited to the first coordination sphere) and probable border effects in the calculation of the atomic potentials with FEFF8.2. Feature D is attributed to the equatorial atoms. Qualitatively, it is shifted to higher energy (49 eV with respect to A) compared to the spectrum of neptunyl hydroxide (38 eV with respect to A), as expected for a contracted equatorial plane.

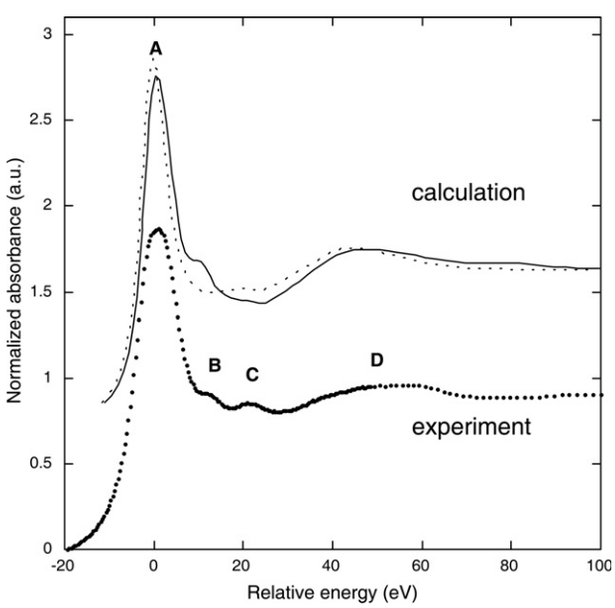

Fig. 7 Experimental and calculated (shifted on the ordinate) L_{III} edge spectra of $[OsO_2(OH)_4]^{2-}$. Two types of calculations are presented: one in the single scattering approach (dotted line), the other one in the full multiple scattering formalism (solid line). The calculation is based on the optimization of the osmium first coordination sphere by quantum chemistry calculations.

Quantum chemical interpretation of the XANES spectra

Several interpretations of the edge spectrum have been proposed using various methods such as multiple scattering, band structure calculations, molecular orbital or multiplet calculations, depending on the system of interest. It is well beyond the scope of this article to review the tremendous amount of work reported in this field. In the case of actinide elements, the large number of electrons involved in the system as well as the partially delocalized character of the 5f states (compared to the 4f ones) complicates the interpretation. At the L_{III} edge, very short core hole lifetimes (7.5 eV for U[66]) preclude the observation of transitions to discrete low lying bound states. On the contrary, excited states in the continuum are intense and broad. Whether the edge or part of the edge should be treated as transitions to discrete bound states depends on the localization of the vacuum level, lying a few electron volts above the HOMO orbital. The interpretation of the white line is often discussed in terms of constructive scattering processes although the atomic contribution is also non-negligible.[28, 31, 33] In this framework, the MO picture and the multiple scattering description are complementary to describe excited states involving bound and mixed bound-continuum states. In this section we propose to relate the edge interpretation to a molecular orbital picture obtained with ADF calculations. On the one hand, the FEFF8.2 code provides information concerning the electronic structure through the calculation of the angular momentum projected local density of states and its relation with the absorption coefficient. On the other hand, from the quantum chemistry code ADF, we have a detailed description of the electronic ground states in term of molecular orbitals. Although the nature of the actinyl bond has been largely described in the literature[6, 67, 68] and often related to optical data when available, little has been done to relate these calculations to the X-ray absorption spectrum.[6]

The valence molecular orbitals of $[UO_2(H_2O)_5]^{2+}$, $[NpO_2(H_2O)_5]^{2+}$ $[NpO_2(OH)_4]^{2-}$ and $[OsO_2(OH)_4]^{2-}$ have been calculated at the DFT level with ADF. The energy and nature of the filled molecular orbitals (MO) having significant participation on the metal ($\geq$10%) are reported on Fig. 8. The MOs are labelled according to the symmetry group corresponding to the calculated structures. The bonding between oxygen and U or Np is due to the donation from the oxygen p orbitals into the empty 6d and 5f orbitals U or Np. For instance, the bonding in neptunyl is very similar to that of uranyl[68] and the extra 5f electron in neptunyl has no overlap with the oxygen orbital. The osmyl bond is mainly characterized by a mixing between Os(5d) and O(2p) orbitals. The participation of the 5d orbitals in the oxo bond is larger than the participation of U and Np 6d's since the Os(5d) contribution reaches nearly 50% in the MO denoted as b_g in Fig. 8. Therefore, the axial distance is shorter for Os (1.75 Å) than for Np (1.82 Å) as shown in Table 1. On the other hand, the Np(6d) contribution to the bonding MOs does not exceed ~20%. As a result of the large Os(5d)/O(2p) mixing, the 5d orbitals spread throughout a large energy range whereas the splitting of the 6d manifold is less important. In all the complexes,

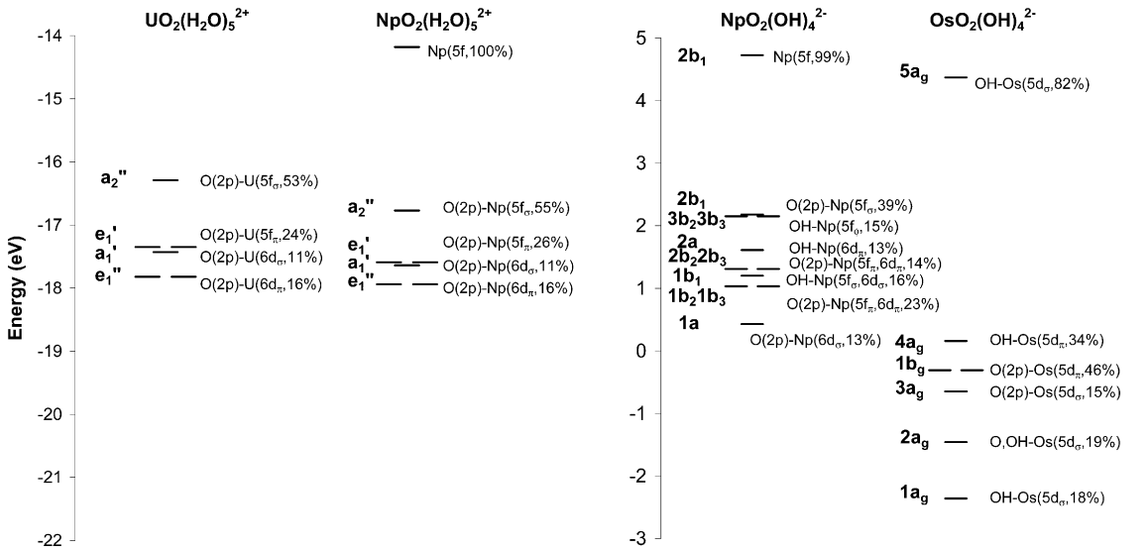

Fig. 8 ADF molecular orbital energies and nature of selected occupied valence orbitals. Only the orbitals having a least 10% contribution on the metal are reported. O refers to the oxo oxygens and the percentage given corresponds to the metal contribution. The MOs are labelled by their symmetries in the symmetry groups of the optimized geometries of the complexes: D_{5h} for $[MO_2(H_2O)_5]^{2+}$, D_2 for $[NpO_2(OH)_4]^{2-}$ and C_{2h} for $[OsO_2(OH)_4]^{2-}$.

the equatorial oxygen atoms of the ligands (H_2O or OH^-) participate also in the bonding. In particular, the OH^- groups make a significant contribution to the bonding and donate electrons into the 5f and 6d orbitals of Np (2a, $3b_2$ and $3b_3$ MOs) and into the 5d orbitals of Os ($1a_g$, $2a_g$and $4a_g$ MOs), as shown on Fig. 8. On the contrary, the water molecules are not as good electron donors as OH^- and no significant mixing between the oxygen atoms of the water and the 5f or 6d orbitals of Np or U is found (the Np or U contribution is less than 10% and is not reported on Fig. 8).

The shape and energy position of the local density of states (f DOS and d DOS of the metal cation) calculated with FEFF8.2 are shown in Fig. 9. They are compared with the MOs calculated with ADF. We should first note that $[MO_2(OH)_4]^{2-}$ complexes are doubly charged and that orbital levels are not rigorously treated at the DFT level for negatively

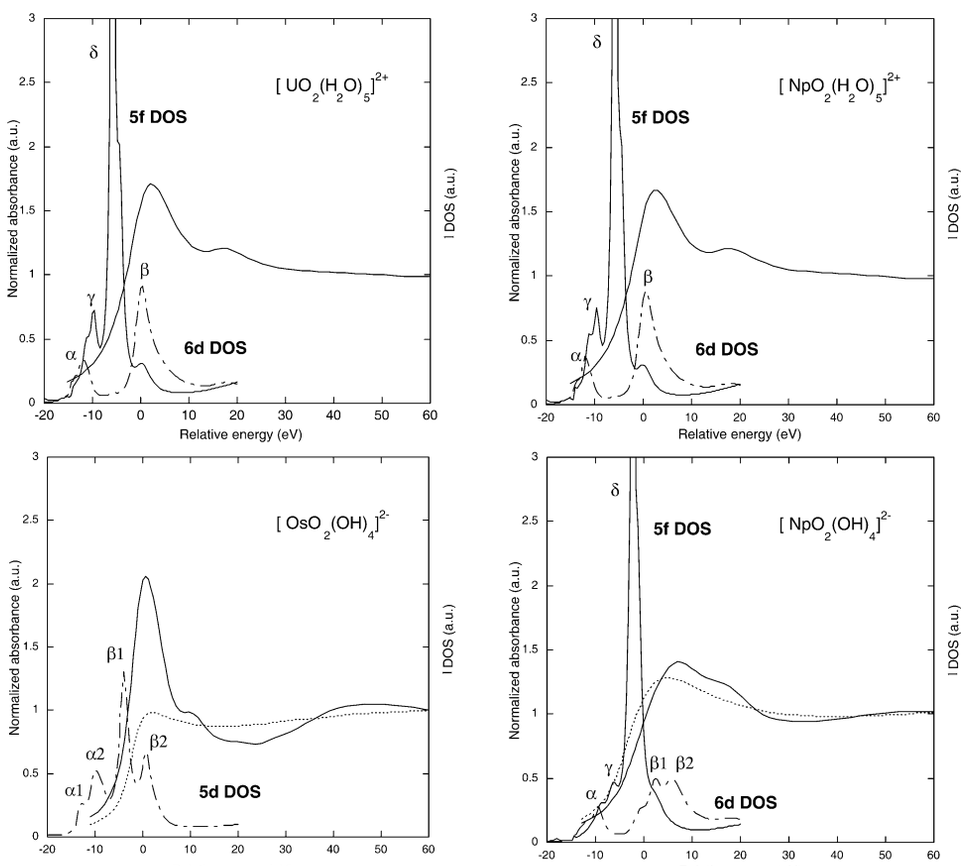

Fig. 9 Calculated *l*-projected DOS and L_{III} edges of $[UO_2(H_2O)_5]^{2+}$, $[NpO_2(H_2O)_5]^{2+}$, $[NpO_2(OH)_4]^{2-}$ and $[OsO_2(OH)_4]^{2-}$. The atomic part of the absorption coefficient μ_{at} is also presented for $[NpO_2(OH)_4]^{2-}$ and $[OsO_2(OH)_4]^{2-}$.

charged species; thus, only a qualitative interpretation should be given to the energy values mentioned here. Given the relation between ρ and μ in the one-electron multiple scattering formalism and the connection between the Green's function formalism and the wave function calculation,[36] an interpretation of the low lying localized states contained in the edge spectrum (although their absolute position in energy is unknown) in terms of MO levels can be attempted. Note that the edge calculations are based on the final state rule and effects of the core hole lifetime are taken into account by broadening of the edge transition. The first peak, labelled α, of the 6d DOS of $[MO_2(H_2O)_5]^{2+}$ (M = U, Np) is associated with the e_1'' and a_1' MOs and corresponds to M(6d)–O_{oxo}(2p) bonding orbitals whereas the second and largest peak β corresponds to the 6d vacant orbitals with density in the equatorial plane. The weak intensity of α is associated with the small contribution of the 6d to the bonding orbitals (less than 20%). The calculated splitting with ADF between the α and β peaks is roughly 9 eV for uranyl and 10 eV for neptunyl while it is 12 eV for both actinyls with FEFF. Concerning the 5f DOS, γ is associated to the to the e_1' and a_2'' MOs [M(5f)–O_{oxo}(2p) bonding orbitals] with the shoulder corresponding to the lowest energy e_1' MO. Peak δ is associated to the 5f orbital that remains localized on U or Np. The γ − δ splitting is evaluated at 3 eV with ADF and at 4 eV with FEFF. From $[NpO_2(H_2O)_5]^{2+}$ to $[NpO_2(OH)_4]^{2-}$, the peaks at low energy of both 6d and 5f DOS (α, γ) become slightly broadened and less intense. This is associated to the increased contribution of the 6d and 5f orbitals to the Np–O_{OH} bonding orbitals in comparison with Np–O_{H_2O} bonds, resulting in an increase of the splitting of the 6d and 5f orbitals. The vacant 6d orbitals in $[NpO_2(OH)_4]^{2-}$ have strong positive values in the DFT calculation and are not meaningful in terms of localized bond states. However, we can assume that the splitting of the β peak into β1 and β2 results from the participation of 6d orbital in the M–O_{OH} bonds.

The structures in the 5d DOS of $[OsO_2(OH)_4]^{2-}$ completely differ from those obtained in the 6d DOS of $[NpO_2(OH)_4]^{2-}$. The major difference between the electronic structures of the two complexes is the larger participation of the 5d orbitals in the bonding in comparison with the 6d ones. This is shown by the population analysis given in Table 2 where ADF and FEFF calculations give both 5 more electrons in the d shell of Os than of Np. At low energy, peak α1 is attributed to the $1a_g$ and $2a_g$ MOs (essentially Os–O_{OH} bonding MOs) and peak α2 to $3a_g$, $1b_g$ and $4a_g$ MOs (Os–O_{oxo} and Os–O_{OH} bonding MOs). The high intensity of peak β1 is associated with the 5d orbitals having no significant overlap with oxygen orbitals ($5a_g$ and low energy vacant 5d orbitals) whereas peak β2 is attributed to the remaining vacant 5d orbital. The calculated value for the α1 − α2 splitting is 3 eV with ADF and FEFF whereas the α2 − β1 splitting is 5 eV with ADF and 6 eV with FEFF. Overall, the shape and the relative positions of the local density of states calculated with FEFF8.2 are consistent with the MO picture. The population analysis of each shell calculated with ADF and FEFF8.2 give also a comparable description of the electronic structure (see Table 2). In particular, ADF and FEFF8.2 give similar evolutions of the population of each electronic shell when going from U to Np and from Np to Os. Although the absolute values for the overall electronic occupation of the metal center are significantly higher with FEFF8.2 than with ADF, these discrepancies are meaningless since charges in ADF and FEFF8.2 are computed according to very different schemes.[37, 54] Finally, a larger splitting of the 6d orbitals induced by the OH^- equatorial ligands in comparison with H_2O is observed from $[NpO_2(H_2O)_5]^{2+}$ to $[NpO_2(OH)_4]^{2-}$. It also corresponds to an elongation of the oxo ligands and therefore a low energy shift of the corresponding multiple scattering feature. The net result is a broadening of the white line for $[NpO_2(OH)_4]^{2-}$. . The white lines corresponding to $[UO_2(H_2O)_5]^{2+}$ and $[NpO_2(H_2O)_5]^{2+}$ are comparable, in agreement with the close similarity of the corresponding electronic structures.

One of the striking differences between Os and U, Np is the more intense white line corresponding to the dipolar transition to the 5d orbitals. Everything else being equal, the atomic interpretation of the width of the white line is known to be related to the core hole lifetime plus the exchange interaction (negligible here at the L_{III} edge) plus the localization of the vacant or semi-vacant 6d (U, Np) or 5d (Os) orbitals.[69, 70] The core hole lifetime is shorter for uranium than for osmium [Γ(U) = 7.4 eV, Γ(Os) = 5.2 eV[66]] and therefore a wider white line is expected for uranium or neptunium. In Fig. 9, the smooth atomic part μ_{at} of the absorption coefficient calculated by FEFF8.2 is also presented. It shows that the atomic origin of the white line is larger for Np than for Os and suggests that significant constructive scattering resonances contribute to the formation of the intense white line. This is in agreement with the more delocalized character of the 5d orbitals *versus* 6d ones as well as the larger occupancy of the 5d compared to the 6d (see Table 2). One assumption is that the $(OsO_2)O_4$ skeleton can be considered as a distorted octahedron (with two distances: 1.75 and 2.03 Å) and triple multiple scattering contributions involving the triangular Os–O_{ax}–O_{eq} paths may contribute to the build-up of the white line. Further multiple scattering calculations should be able to valid this assumption.

Conclusion

Although the L_{III} X-ray absorption edges of actinyl compounds have been intensively investigated, the comprehensive understanding of the underlying electronic phenomena is still partial. In this paper, three actinyl compounds and one equivalent in the d block family have been taken as examples: $[UO_2(H_2O)_5]^{2+}$, $[NpO_2(H_2O)_5]^{2+}$ $[NpO_2(OH)_4]^{2-}$ and $[OsO_2(OH)_4]^{2-}$. Edge calculations using the multiple scattering formalism of FEFF8.2 have been performed based on clusters obtained by molecular dynamics calculations. Such calculations show that the role of the solvent (here water) is important in order to better describe the atomic potentials of the cation first coordination sphere. On the other hand, the influence on the edge shape of the atoms beyond the oxygen atoms of the first coordination sphere is negligible. Comparison between $[NpO_2(H_2O)_5]^{2+}$ and $[NpO_2(OH)_4]^{2-}$ shows the sensitivity of the position and intensity of the edge features

Table 2 Mulliken population analysis of the metal centers with ADF and FEFF8.2

	ADF				FEFF8.2			
	s	p	d	f	s	p	d	f
$[UO_2(H_2O)_5]^{2+}$	0.00	5.65	1.36	2.61	0.31	6.05	2.00	3.53
$[NpO_2(H_2O)_5]^{2+}$	0.00	5.61	1.31	3.79	0.31	6.05	1.95	4.71
$[NpO_2(OH)_4]^{2-}$	0.04	5.76	1.45	3.70	0.37	6.07	1.94	4.76
$[OsO_2(OH)_4]^{2-}$	0.23	0.16	5.35	0.01	0.64	0.86	6.46	0.00

to slight distortions of the molecular skeleton. Above the edge maximum, an interpretation in terms of multiple scattering contributions originating from the axial trans dioxo bond is given. In a second step, a tentative interpretation of the edge in terms of the *l*-projected density of states as well as molecular orbital levels from ADF calculations is presented. Clearly, the attribution of the edge feature or part of the edge to bound or quasi-bond final states *versus* continuum states is difficult. The interpretation given here shows that a relatively satisfactory agreement is found between the MO levels and the DOS calculations related to the low lying states of the edge spectrum. It also qualitatively corroborates the quantum chemical analysis of the cation–oxygen bonds within the molecular skeleton. Finally, a comparison between the edges of $[NpO_2(OH)_4]^{2-}$ and $[OsO_2(OH)_4]^{2-}$ shows a strong discrepancy in the white line intensity. Although the broadening of the core hole lifetime is larger for Np than for Os it is assumed, by comparison of the atomic absorption coefficients, that additional multiple scattering resonances contribute to the osmium white line intensity.

Acknowledgements

All experimental measurements were performed at the Stanford Synchrotron Radiation Laboratory, a national user facility operated by Stanford University on behalf of the U.S. Department of Energy, Office of Basic Energy Sciences. The authors would like to thank for their help J. Bargar and J. Rogers at the SSRL/11-2. Health Physics support was provided by the Los Alamos National Laboratory section of the Seaborg Institute for Transactinium Studies. This work was supported by CEA (France), PRACTIS (France) and the NNSA and OBES Division of Chemical Sciences under Contract W-7405 (USA).

References

1 N. M. Edelstein, *J. Alloys Compd.*, 1995, **223**, 197.
2 C. Gorller-Walrand and L. G. Vanquickenborne, *J. Chem. Phys.*, 1970, **54**, 1436.
3 M. Boring, J. H. Wood and J. W. Moskowitz, *J. Chem. Phys.*, 1975, **63**, 638.
4 R. L. Dekock, E. J. Baerends, P. M. Boerrigter and J. G. Snijders, *Chem. Phys. Lett.*, 1984, **105**, 308.
5 C. Clavaguéra-Sarrio, V. Brenner, S. Hoyau, C. J. Marsden, P. Millié and J.-P. Dognon, *J. Phys. Chem. B*, 2003, **107**, 3051.
6 R. G. Denning, J. C. Green, T. E. Hutchings, C. Dallera, A. Tagliaferri, K. Giarda, N. B. Brookes and L. Braicovich, *J. Chem. Phys.*, 2002, **117**, 8008.
7 R. Denning, *Struct. Bonding*, 1992, **79**, 215.
8 G. Meinrath, U. Kato and Z. Yoshida, *J. Radioanal. Nucl. Chem.*, 1993, **174**, 299.
9 K. Yoshiharu, G. Meinrath, T. Kimura and Z. Yoshida, *Radiochim. Acta*, 1994, **64**, 107.
10 G. Meinrath, U. Kato, T. Kimura and Z. Yoshida, *Radiochim. Acta*, 1999, **84**, 21.
11 I. Billard, A. Rustenholtz, L. Sémon and K. Lützenkirchen, *Chem. Phys.*, 2001, **270**, 345.
12 A. Rustenholtz, I. Billard, G. Duplâtre, K. Lützenkirchen and L. Sémon, *Radiochim. Acta*, 2001, **89**, 83.
13 B. Barker, R. Denning and J. Thorne, *Inorg. Chem.*, 1987, **26**, 1721.
14 C. Görller-Walrand and S. Dejagere, *Spectrochim. Acta, Part A*, 1972, **28**, 257.
15 C. Görller-Walrand, W. Colen and N. Dao, *J. Chem. Phys.*, 1982, **76**, 13.
16 C. Jorgensen and R. Reisfeld, *Struct. Bonding*, 1982, **50**, 121.
17 R. Denning, T. Sneellgrove and D. Woodwark, *Mol. Phys.*, 1976, **32**, 419.
18 R. Denning, D. Foster, T. Sneellgrove and D. Woodwark, *Mol. Phys.*, 1979, **37**, 1089.
19 R. Denning, T. Sneellgrove and D. Woodwark, *Mol. Phys.*, 1979, **37**, 1109.
20 P. F. Walch and D. E. Ellis, *J. Chem. Phys.*, 1976, **65**, 2387.
21 J. Krupa, E. Simoni, J. Systma and N. Edelstein, *J. Alloys Compd.*, 1994, **213/214**, 471.
22 L. Sémon, C. Boehme, I. Billard, C. Hennig, K. Lützenkirchen, T. Reich, A. Robberg, I. Rossini and G. Wipff, *Chem. Phys. Chem.*, 2001, **2**, 591.
23 V. Vallet, U. Wahlgren, B. Schimmelpfennig, H. Moll, Z. Szabò and I. Grenthe, *Inorg. Chem.*, 2001, **40**, 3516.
24 D. L. Clark, S. D. Conradson, R. J. Donohoe, D. W. Keogh, D. E. Morris, P. D. Palmer, R. D. Rogers and C. D. Tait, *Inorg. Chem.*, 1999, **38**, 1456.
25 H. Bolvin, U. Wahlgren, H. Moll, T. Reich, G. Geipel, T. Fanghanel and I. Grenthe, *J. Phys. Chem. A*, 2001, **105**, 11 441.
26 S. D. Conradson, *Appl. Spectrosc.*, 1998, **52**, 252.
27 T. Reich, G. Bernhard, G. Geipel, H. Funke, C. Hennig, A. Rossberg, W. Matz, N. Schell and H. Nitsche, *Radiochim. Acta*, 2000, **88**, 633.
28 A. L. Ankudinov, S. D. Conradson, J. Mustre de Leon and J. J. Rehr, *Phys. Rev. B*, 1998, **57**, 7518.
29 E. A. Hudson, P. G. Allen, L. J. Terminello, M. A. Denecke and T. Reich, *Phys. Rev. B*, 1996, **54**, 156.
30 E. A. Hudson, J. J. Rehr and J. J. Bucher, *Phys. Rev. B*, 1995, **52**, 13 815.
31 C. Den Auwer, E. Simoni, S. D. Conradson, J. Mustre de Leon, P. Moisy and A. Béres, *C. R. Acad. Sci., Ser. IIc: Chim.*, 2000, **3**, 327.
32 M. Sandström, I. Persson, F. Jalilehvand, P. Lindquist-Reis, D. SpÅngberg and K. Hermansson, *J. Synchotron Radiat.*, 2001, **8**, 657.
33 S. D. Conradson, K. D. Abney, B. D. Begg, E. D. Brady, D. L. Clark, C. Den Auwer, M. Ding, P. K. Dorhout, F. J. Espinosa, P. L. Gordon, R. G. Haire, N. J. Hess, R. F. Hess, D. W. Keogh, G. H. Lander, A. J. Lupinetti, L. A. Morales, M. P. Neu, P. D. Palmer, P. Paviet, S. D. Reilly, W. H. Runde, C. D. Tait, D. K. Veirs and F. Wastin, *Inorg. Chem.*, 2004, **43**, 116.
34 A. L. Ankudinov, B. Ravel, J. J. Rehr and S. D. Conradson, *Phys. Rev. B*, 1998, **58**, 7565.
35 A. Filipponi, *J. Phys.: Condens. Matter*, 2001, **13**, R23.
36 H. Modrow, S. Bucher, J. J. Rehr and A. L. Ankudinov, *Phys. Rev. B*, 2003, **67**, 35 123.
37 J. J. Rehr and R. C. Albers, *Rev. Mod. Phys.*, 2000, **72**, 621; M. Newville, *J. Synchrotron Radiat.*, 2001, **8**, 322.
38 C. Den Auwer, R. Drot, E. Simoni, S. D. Conradson, M. Gailhanou and J. Mustre de Leon, *New J. Chem.*, 2003, **27**, 648.
39 D. W. Keogh, D. L. Clark and S. D. Conradson, personal communication.
40 J. Malin and H. Taube, *Inorg. Chem.*, 1971, **10**, 2403.
41 C. W. Williams, J.-P. Blaudeau, J. C. Sullivan, M. R. Antonio, B. Bursten and L. Soderholm, *J. Am. Chem. Soc.*, 2001, **123**, 4346.
42 D. A. Case, D. A. Pearlman, J. W. Caldwell, T. E. Cheatham III, W. S. Ross, C. L. Simmerling, T. A. Darden, K. M. Merz, R. V. Stanton, A. L. Cheng, J. J. Vincent, M. Crowley, V. Tsui, R. J. Radmer, Y. Duan, J. Pitera, I. Massova, G. L. Seibel, U.C. Singh, P. K. Weiner and P. A. Kollman, *AMBER 6*University of California, San Francisco, CA, USA, 1999.
43 D. A. Pearlman, D. A. Case, J. W. Cadwell, W. S. Ross, T. E. Cheatham III, S. Debolt, D. M. Ferguson, G. L. Seibel and P. A. Kollman, *Comp. Phys. Commun.*, 1995, **91**, 1.
44 P. Guilbaud and G. Wipff, *J. Phys. Chem.*, 1993, **97**, 5685.
45 P. Guilbaud and G. Wipff, *J. Inclusion Phenom. Mol. Recognit. Chem.*, 1993, **16**, 169.
46 P. Guilbaud and G. Wipff, *J. Mol. Struct. (THEOCHEM)*, 1996, **366**, 55.
47 P. Guilbaud and G. Wipff, *New J. Chem.*, 1996, **20**, 631.
48 F. Hutschka, A. Dedieu, L. Troxler and G. Wipff, *J. Phys. Chem. A*, 1998, **102**, 3773.
49 M. J. Frisch, G. W. Trucks, H. B. Schlegel, G. E. Scuseria, M. A. Robb, J. R. Cheeseman, V. G. Zakrzewski, J. A. Montgomery, Jr., R. E. Stratmann, J. C. Burant, S. Dapprich, J. M. Millam, A. D. Daniels, K. N. Kudin, M. C. Strain, O. Farkas, J. Tomasi, V. Barone, M. Cossi, R. Cammi, B. Mennucci, C. Pomelli, C. Adamo, S. Clifford, J. Ochterski, G. A. Petersson, P. Y. Ayala, Q. Cui, K. Morokuma, D. K. Malick, A. D. Rabuck, K. Raghavachari, J. B. Foresman, J. Cioslowski, J. V. Ortiz, B. B. Stefanov, G. Liu, A. Liashenko, P. Piskorz, I. Komaromi, R. Gomperts, R. L. Martin, D. J. Fox, T. Keith, M. A. Al-Laham, C. Y. Peng, A. Nanayakkara, C. Gonzalez, M. Challacombe, P. M. W. Gill, B. G. Johnson, W. Chen, M. W. Wong, J. L. Andres, M. Head-Gordon, E. S. Replogle and J. A. Pople,

GAUSSIAN 98 (Revision A.9), Gaussian, Inc., Pittsburgh, PA, 1998.
50 C. I. Bayly, P. Cieplak, W. D. Cornell and P. A. Kollman, *J. Phys. Chem.*, 1993, **97**, 10 269.
51 T. Harden, D. York and L. Pedersen, *J. Chem. Phys.*, 1993, **98**, 10 089.
52 G. te Velde, F. M. Bickelhaupt, S. A. J. van Gisbergen, C. Fonseca Guerra, E. J. Baerends, J. G. Snijders and T. Ziegler, *J. Comput. Chem.*, 2001, **22**, 931.
53 C. Fonseca Guerra, J. G. Snijders, G. te Velde and E. J. Baerends, *Theor. Chem. Acc.*, 1998, 391.
54 In *ADF2002.03*, SCM, Theoretical Chemistry, Vrije Universiteit, Amsterdam, The Netherlands, 2002 (http://www.scm.com).
55 E. van Lenthe, A. Ehlers and E. J. Baerends, *J. Chem. Phys.*, 1999, **110**, 8943.
56 E. van Lenthe, E. J. Baerends and J. G. Snijders, *J. Chem. Phys.*, 1993, **99**, 4597.
57 E. van Lenthe, E. J. Baerends and J. G. Snijders, *J. Chem. Phys.*, 1994, **101**, 9783.
58 J. P. Perdew, J. A. Chevary, S. H. Vosko, K. A. Jackson, M. R. Pederson, D. J. Singh and C. Fiolhais, *Phys. Rev. B*, 1992, **46**, 6671; S. H. Vosko, L. Wilk and M. Nusair, *Can. J. Phys.*, 1980, **58**, 1200.
59 Y. Oda and A. Aoshima, *J. Nucl. Sci. Technol.*, 2002, **39**, 647.
60 C. Den Auwer, E. Simoni, S. D. Conradson and C. Madic, *Eur. J. Inorg. Chem.*, 2003, **21**, 3843.
61 M. Benfatto, S. D. Longa and R. C. Natoli, *J. Synchotron Radiat.*, 2003, **10**, 51.
62 P. J. Merkling, A. Muñoz-Páez and E. Sánchez Marcos, *J. Am. Chem. Soc.*, 2002, **124**, 10 911.
63 P. J. Merkling, A. Muñoz-Páez, R. R. Pappalardo and E. Sánchez Marcos, *Phys. Rev. B*, 2001, **64**, 2201.
64 P. D'Angelo, V. Barone, G. Chillemi, N. Sanna, W. Meyer-Klauche and N. V. Pavel, *J. Am. Chem. Soc.*, 2002, **124**, 1958.
65 C. Den Auwer, S. D. Conradson, P. Guilbaud, P. Moisy, J. Mustre de Leon and E. Simoni, in *Proccedings of the XAFS XII Conference, Malmö, Sweden*, accepted for publication.
66 M. O. Krause and J. H. Oliver, *J. Phys. Chem. Ref. Data*, 1979, **8**, 329.
67 J. S. Craw, M. A. Vincent, I. H. Hillier and A. L. Wallwork, *J. Phys. Chem.*, 1995, **99**, 10 181.
68 S. Matsika and R. M. Pitzer, *J. Phys. Chem. A*, 2000, **104**, 4064.
69 G. Kalkowski, G. Kaindl, W. D. Brewer and W. Krone, *Phys. Rev. B*, 1987, **35**, 2667.
70 J. Petiau, G. Calas, D. Petitmaire, A. Bianconi, M. Benfatto and A. Marcelli, *Phys. Rev. B*, 1986, **34**, 7350.